Low-Frequency Variability of Temperature in the Vicinity of the Equatorial Pacific Thermocline in SODA: Role of Equatorial Wave Dynamics and ENSO Asymmetry

B. Dewitte, S. Thual, S. W. Yeh, S. I. An, B. K. Moon, B. S. Giese

NOTES AND CORRESPONDENCE

Low-Frequency Variability of Temperature in the Vicinity of the Equatorial Pacific Thermocline in SODA: Role of Equatorial Wave Dynamics and ENSO Asymmetry

B. DEWITTE,*,+ S. THUAL,+,# S.-W. YEH,@ S.-I. AN,& B.-K. MOON,** AND B. S. GIESE++

* *Laboratoire d'Etude en Géophysique et Océanographie Spatiale, Toulouse, France*
+ *Instituto del Mar del Peru, Callao, Peru*
# *ENSEEIHT, Toulouse, France*
@ *Korea Ocean Research and Development Institute, Ansan, South Korea*
& *Department of Atmospheric Sciences, Global Environmental Laboratory, Yonsei University, Seoul, South Korea*
** *Division of Science Education, Institute of Science Education, Chonbuk National University, Jeonju, South Korea*
++ *Department of Oceanography, Texas A&M University, College Station, Texas*

(Manuscript received 31 July 2008, in final form 29 April 2009)

ABSTRACT

The Simple Ocean Data Assimilation (SODA) reanalysis (1958–2001) is used to investigate the decadal variability in the equatorial thermocline in the Pacific. Whereas the thermocline depth exhibits weak variation at decadal time scales, the temperature change in the vicinity of the thermocline in the western Pacific is significant and has a vertical scale of ~150 m. Based on a modal decomposition of the model variability, it is shown that such temperature change can be interpreted to a large extent as vertical displacements of the isotherms associated with the Kelvin and first meridional Rossby waves of the first three baroclinic modes. This indicates that decadal change at the subsurface in the warm pool region may be forced by the winds, consistent with the results of a multimode linear model simulation. The decadal mode of vertical temperature can be described by the first two dominant statistical modes (EOFs): the first mode is associated with changes in the slope of the thermocline (swallowing in the western-central Pacific and deepening in the eastern Pacific), representative of the 1976/77 climate shift and ahead of the ENSO modulation; and the second mode corresponds to a basinwide uplift of the thermocline and behind the ENSO modulation. It is further shown that the subsurface temperature in the warm pool region is negatively skewed, which results from the ENSO asymmetry. The results are consistent with the hypothesis of change in mean state resulting from the residual effect of the asymmetric ENSO variability.

1. Introduction

The issue of the source of the ENSO modulation in the tropical Pacific has drawn considerable interest in recent years. Indeed, it has not been clear to what extent the change in ENSO characteristics at decadal time scale is due to external forcing [from the atmosphere through the teleconnections (Pierce et al. 2000) or from the ocean through the oceanic tunnels (Gu and Philander 1997; Luo and Yamagata 2001; Giese et al. 2002; Luo et al. 2003; Moon et al. 2007)], or if the ENSO equatorial dynamics can produce its own decadal variability through nonlinearities (Timmermann and Jin 2002; Timmermann 2003; Rodgers et al. 2004; Yeh and Kirtman 2004; Dewitte et al. 2007; Burgman et al. 2008). Others have argued that the ENSO modulation could also result from noise forcing (Blanke et al. 1997; Yeh and Kirtman 2008). The difficulty in addressing such an issue lies in part with the fact that the equatorial thermocline exhibits relatively weak variability at decadal time scales (less than ~5 m in the central Pacific; Wang and An 2001), which limits the significance of statistical analysis or the interpretation of sensitivity tests from models in studies addressing the issue of the effect of change in mean equatorial thermocline depth on the ENSO modulation for instance. The little changes in thermocline depth, usually approximated at the 20°C isotherm depth, does not mean, however, that temperature changes in the vicinity of the

Corresponding author address: Boris Dewitte, IRD-Lima, 357 Calle Teruel, Miraflores, Peru.
E-mail: boris.dewitte@gmail.com

DOI: 10.1175/2009JCLI2764.1

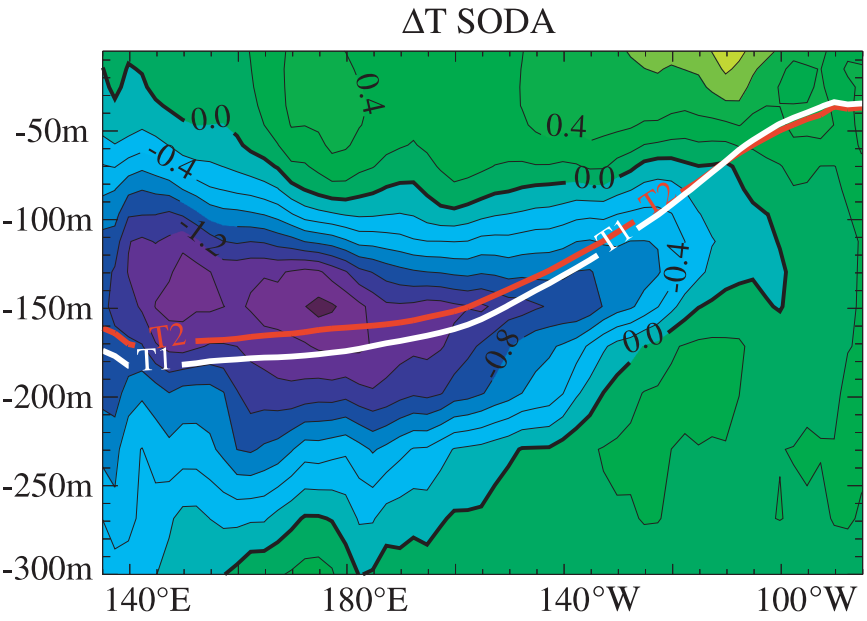

FIG. 1. Temperature difference between the mean during the period 1980–97 and the mean during the period 1958–75 as a function of longitude and depth along the equator. The contour interval is 0.2°C. The mean depth of the 20°C isotherm over the two periods is also plotted (red, 1980–97; white, 1958–75).

thermocline are not marked. In particular, Moon et al. (2004) showed from the so-called Simple Ocean Data Assimilation (SODA) dataset (Carton et al. 2000) that cooling at subsurface occurred after the 1976/77 climate shift (Guilderson and Schrag 1998) along the equator, which reaches 1.4°C in the western equatorial Pacific at ~150 m with a vertical scale of ~100 m (their Fig. 1d). From intermediate coupled model experiments, they further show that such cooling has the potential of affecting the equatorial wave dynamics toward more intense and "slower" ENSO. Figure 1 displays the temperature change along the equator associated with the 1976/77 climate shift. This figure is equivalent to Fig. 1d of Moon et al. (2004), except that our Fig. 1 uses a more recent version of SODA (Carton and Giese 2008). As with Moon et al. (2004), it indicates that the cooling pattern has a vertical scale of the order of ~150 m and is centered in the western-central Pacific. The mean thermocline depth for the periods before and after the 1976/77 shift is also displayed, which indicates that it experienced a change of no more than 10 m between the two periods. Such a pattern indicates that an increase in ENSO variability (as it occurred after the 1970s), and hence an overall warming of the surface layer, is associated with a cooling at the subsurface that encompasses a significant part of the warm pool along the equator (~50%). In addition, this cooling at the subsurface is much more intense (in absolute value) than its "warm" counterpart in the surface layers. Thus, the average warming along the equator associated with the 1976/77 climate shift in the first 100 m is ~0.31°C, whereas the average cooling in the 100–250-m-depth range reaches approximately −0.60°C. Then questions arise from such observations, including, what is the process associated with such cooling? Does it result from a change in equatorial wave dynamics? What process determines the large vertical extent of the temperature anomaly around the thermocline? More generally, how is it related to the change in ENSO variability?

This paper attempts to reply to these questions; it can be viewed as an extension of the Moon et al. (2004) paper in the sense that, instead of focusing on the impact of change in mean state on ENSO characteristics, it questions if the ENSO modulation can lead to change in mean state similar to what is observed from a reanalysis product. In addition to its modulation, the paper also considers another recently documented important characteristic of ENSO: its asymmetry, namely, its tendency to produce stronger El Niño events than La Niña events (An and Jin 2004). From surface observations, there is evidence that this so-called ENSO asymmetry is tightly linked to the change in mean state (An 2004, 2008). Recent model studies also support this hypothesis, whether they are based on a rather simple conceptual approach (Timmermann and Jin 2002; Schopf and Burgman 2006) or on full complexity models (Rodgers

et al. 2004; Yeh and Kirtman 2004; Cibot et al. 2005; Dewitte et al. 2007). In the light of these results, the focus here is given on subsurface temperature change in the vicinity of the equatorial thermocline and their interpretation in terms of equatorial wave dynamics. A vertical mode decomposition of the SODA outputs is carried out and the temperature change associated with the gravest baroclinic modes is estimated and documented. Because these modes control the ENSO dynamics to a large extent, their contributions to temperature change that are estimated in this paper provide insights into how ENSO distributes the heat vertically in the warm pool region. Recent studies have indirectly addressed this issue from coupled general circulation model (CGCM) outputs. For instance, Moon et al. (2007) have investigated the relationship between vertical mode variability along the equator (as measured by the projection coefficient of the winds) and the variability in the southwestern Pacific at decadal time scales. Dewitte et al. (2007) also documented the role of the high-order baroclinic modes in modulating the ENSO variability through their impact on the nonlinear advection. Here, the aim is first to verify from a more realistic simulation to what extent subsurface variability associated with change in mean state can be interpreted in terms of equatorial waves of the high-order baroclinic modes. In particular, the actual contribution of the baroclinic modes to the change in mean state is diagnosed here through what is referred in the paper as ''baroclinic temperature.'' Second, compared to previous studies, this paper further documents the forcing mechanisms of the change in mean thermocline in the western-central Pacific rather than the impact of the latter on the ENSO variability. In that sense, it complements the formerly mentioned modeling studies.

The paper is organized as follows: Section 2 describes the dataset and method. Section 3 presents the results of the vertical mode decomposition of the decadal signal observed in the SODA reanalysis. Section 4 investigates the relationship between the ENSO modulation and decadal pattern for temperature as a function of depth identified earlier. Section 5 provides a discussion followed by concluding remarks.

2. Data and method

a. SODA

The SODA reanalysis project, which began in the mid-1990s, is an ongoing effort to reconstruct historical ocean climate variability on space and time scales similar to those captured by the atmospheric reanalysis projects. In this paper, we used SODA, version 1.4.2. SODA 1.4.2 uses a general circulation ocean model based on the Parallel Ocean Program numerics (Smith et al. 1992), with an average 0.25° (lat) × 0.4° (lon) horizontal resolution and 40 vertical levels with 10-m spacing near the surface. The constraint algorithm is based on optimal interpolation data assimilation. Assimilated data includes temperature (T) and salinity (S) profiles from the World Ocean Database 2001 [Conkright et al. 2002; mechanical BT (MBT), XBT, CTD, and station data], as well as additional hydrography, SST, and altimeter sea level. The model was forced by daily surface winds provided by the 40-yr European Centre for Medium-Range Weather Forecasts Re-Analysis (ERA-40; Uppala et al. 2005) for the 44-yr period from January 1958 to December 2001. Surface freshwater flux for the period 1979 to the present are provided by the Global Precipitation Climatology Project monthly satellite–gauge merged product (Adler et al. 2003) combined with evaporation obtained from the same bulk formula used to calculate latent heat loss. Sea level is calculated prognostically using a linearized continuity equation, valid for small ratios of sea level to fluid depth (Dukowicz and Smith 1994). Refer to Carton et al. (2000) and Carton and Giese (2008) for a detailed description of the SODA system.

b. Method: Definition of baroclinic temperature

The vertical modes were calculated in a similar way to the method used by Dewitte et al. (1999). The reader is invited to refer to this work for more technical details. To derive the vertical modes, usually, the mean stratification is used. Here, to take into account that there is a change in mean temperature and salinity at low frequency, we added to the mean the low-frequency part of the anomalies (using a 7-yr low-pass filter). The vertical mode decomposition was therefore performed at each time step from the SODA salinity and temperature averaged over the 44 years, on which the 7-yr low-pass-filtered signal was superimposed. Kelvin and first meridional mode Rossby wave contributions to the sea level anomaly are then derived by projecting the pressure and zonal current baroclinic contributions onto the theoretical meridional modes.

Changes in the pressure field induce vertical displacement of the isotherms, resulting in temperature anomalies at a particular depth. With $p(x, y, z, t) = \sum_{n=1}^{M} p_n(x, y, t) \times F_n(x, z, t')$—where p is the pressure field, $p_n(x, y, t)$ is the associated n baroclinic mode contribution, and F_n is the vertical structure of the nth baroclinic mode along the equator associated to the low-frequency change in density (t' stands for the time relative to the low-frequency change in S and T)—the hydrostatic relation leads to $\delta\rho = -\rho_0 \sum_{n=1}^{M} sl_n \times \partial_z(F_n)$, where ρ is

the density and sl_n are the n baroclinic mode contribution to sea level anomalies ($sl_n = p_n/\rho_0 g$). Using the stability equation for the density field and assuming that the density changes (at constant depth) are governed by temperature changes (i.e., $\delta\rho = -\rho\alpha_T\delta T$, with $\alpha_T = 2.97 \times 10^{-4}$ K^{-1}; Gill 1982), a baroclinic temperature can be defined as follows:

$$T_M(x, y, z, t) = \alpha_T^{-1} \sum_{n=1}^{M} sl_n(x, y, t) \frac{dF_n(x, z, t')}{dz}. \quad (1)$$

Note that near the surface, a large number of baroclinic modes are required to correctly account for the small vertical scales in the variability. Thus, the baroclinic temperature will not be representative of temperature change in the surface layers unless a relatively large number of baroclinic modes are retained. For instance, Illig and Dewitte (2006) used a similar methodology to parameterized temperature changes at the base of the mixed layer in an intermediate coupled model of the tropical Atlantic. They found that a total of six baroclinic modes is required to simulate properly the entrainment temperature in the equatorial Atlantic. Because the focus in this study is on temperature variability in the vicinity of the thermocline, we expect that fewer baroclinic modes are required to represent the vertical scales of temperature variability. This assumption ignores that the thermocline in the equatorial Pacific is deeper than in the equatorial Atlantic, which also affects the vertical mode structures.

Notice that, from Eq. (1), one can also derive the Kelvin and Rossby contribution to temperature changes because

$$sl_n(x, y, t) = ak_n(x, t)\Psi_{o,n}(y, x, t') + r_{1,n}(x, t)R^h_{1,n}(x, y, t') + \sum_{j=2}^{\infty} r_{j,n}(x, t)R^h_{j,n}(x, y, t'),$$

where ak_n and $r_{1,n}$ are the Kelvin and first meridional Rossby wave coefficient for the nth baroclinic mode, respectively. Here, $\psi_{o,n}$ and $R^h_{j,n}$ are the meridional structures for the Kelvin and jth meridional mode Rossby wave, respectively, and depend on the baroclinic mode order n.

A baroclinic temperature associated with Kelvin and Rossby waves is then defined as follows:

$$T_M^{K-R1} = \alpha_T^{-1} \sum_{n=1}^{M} (ak_n\psi_{0,n} + r_{1,n}R^h_{1,n}) \frac{dF_n}{dz}.$$

3. Baroclinic mode contributions to vertical temperature variability

a. The 1976 climate shift

Following the method detailed in section 2, temperature variability associated with the baroclinic modes (T_m) is estimated along the equator for the first 300 m. Figures 2a–c are the same as Fig. 1, except for the contribution of the first 10 baroclinic modes, the contribution of the first 3 baroclinic modes, and the summed-up contribution of modes 4–10. Figure 2a indicates that the first 10 baroclinic modes are able to capture the main feature of the pattern of Fig. 1, namely, a cooling in the vicinity of the thermocline in the western-central Pacific with a vertical scale of the order of ~200 m. For the first three baroclinic modes, the obtained pattern consists of a zonal seesaw of temperature anomaly: a marked cooling west of 130°W and a slight warming east of this longitude. Although the surface layer does not experience a warming associated with the 1976 climate shift compared to Fig. 1, resulting in larger vertical scale of the cooling pattern, the core of the cooling pattern still resembles the one of Fig. 1, with a minimum amplitude just above the mean thermocline in the western-central Pacific. This indicates that the cooling above the thermocline associated with the 1976 climate shift can be explained to a large extend by the first three baroclinic modes. Note that the percentage of variance in the Niño-4z region (150°E–150°W; 100–150 m) explained by $\sum_{m=1}^{3} T_m$ reaches 67% (see Table 1). Most of the $\sum_{m=1}^{3} T_m$ variance is associated with the Kelvin and first meridional Rossby mode contributions, as shown in Fig. 2d. The Table 1 summarizes the statistics.

As expected, the pattern for contributions of modes 4–10 exhibits finer vertical scales: it apparently captures the vertical displacements of the mean thermocline with an elongated zone of cooling (warming) along (above) the mean thermocline from west to east. Because high-order modes tend to be trapped within the mixed layer (because of their fine vertical scales and their slow propagating speed), they are associated to a large extent with the local wind stress forcing. In that sense, the pattern associated with modes 4–10, consisting of a uniform cooling/warming near the thermocline, suggests that it is linked to the theoretically very low-frequency (VLF) basin mode proposed by Jin (2001) that has a uniform zonal structure.

Only the first three baroclinic modes will be considered in the rest of the paper: the motivations for this are twofold: 1) they explained a large amount of variance in the Niño-4z region where we focus our interest, and 2) the vertical scale of variability that matters in this study are of the order of ~200 centered around 150 m, which can only

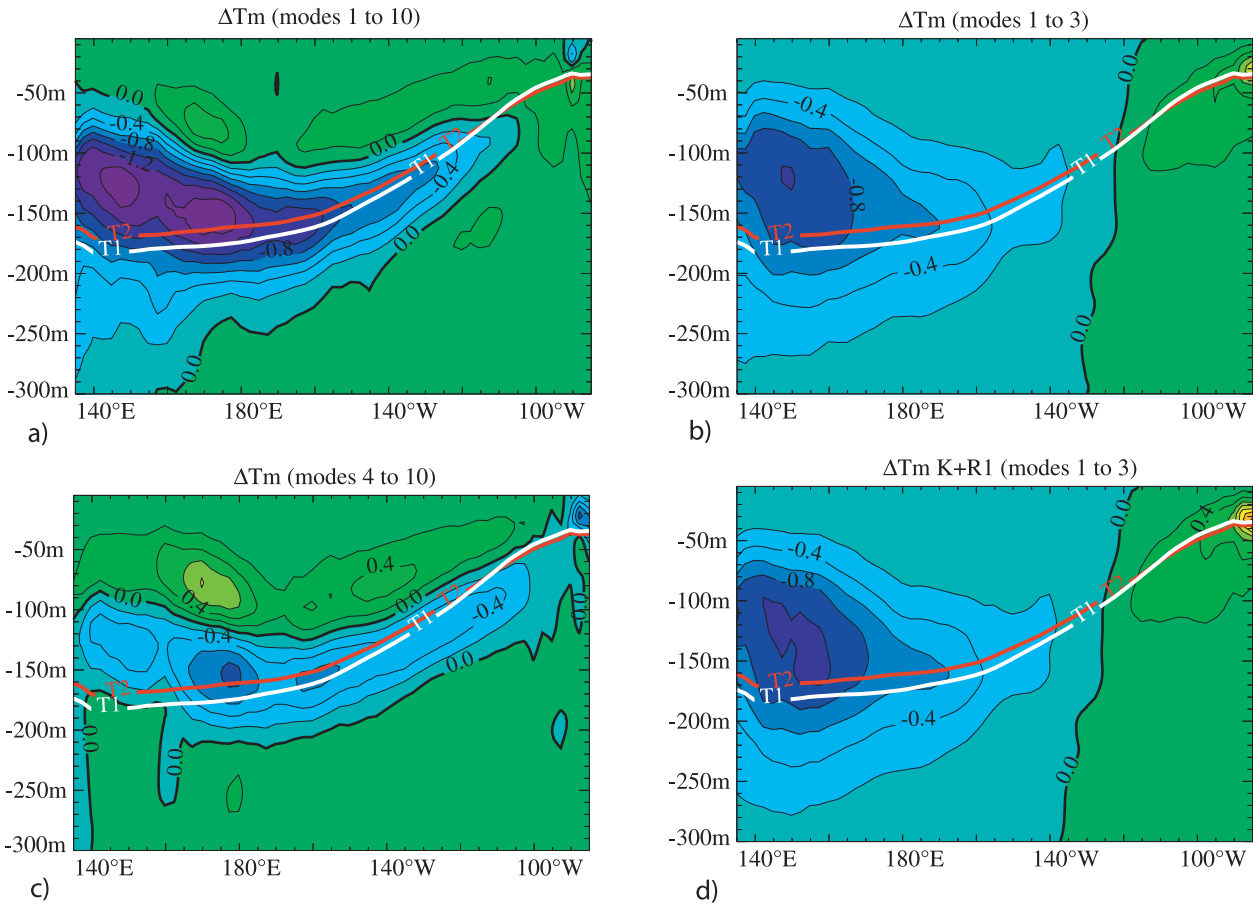

FIG. 2. Same as in Fig. 1, but for the summed-up contribution of the baroclinic modes (a) 1–10 (b) modes 1–3, (c) modes 4–10, and (d) for the contribution of the Kelvin and first meridional Rossby waves of the first three baroclinic modes.

be accounted for by the gravest baroclinic modes (higher-order mode having too fine vertical scales to account for such vertical structure variability). Notice that the first three baroclinic modes are the most relevant for the study of ENSO dynamics (Dewitte 2000; Yeh et al. 2001) and are more than likely involved in the mechanism of rectification of ENSO by change in mean state (Dewitte et al. 2007).

b. Decadal variability

In this paragraph, the above results are generalized and extended by focusing on the decadal variability of equatorial temperature in the upper 300 m instead of just the change in temperature associated with the 1976 climate shift. To do so, an EOF analysis on the vertical section of temperature along the equator is performed after low-pass filtering the data. A frequency cutoff at 7 $(\text{yr})^{-1}$ is used for the filter. The results are presented in Fig. 3 for the first two dominant modes. A Monte Carlo test was carried out to check the significance of the EOF patterns following Björnsson and Venegas (1997). The method consists of creating a surrogate data, a randomized dataset of $T(x, z, t)$ by scrambling the monthly maps of 40 years (selected among the 54 years of the SODA data) in the time domain. The scrambling is performed on the year and not on the months to maintain the order of the months inside the year. The EOF analysis is then performed on the scrambled dataset. The same procedure of scrambling the dataset and performing the analysis is repeated 100 times, each time keeping the

TABLE 1. Percentage of variance in the Niño-4z region (150°E–150°W; 100–150 m) explained by $\sum T_m$.

Percent of explained variance	Modes 1–3 (%)	Modes 1–10 (%)
$\sum_m T_m / T_{\text{SODA}}$	67	99
$\sum_m T_m^{K-R1} \Big/ \sum_m T_m$	105	—
$\sum_m T_m^{K} \Big/ \sum_m T_m$	74	—
$\sum_m T_m^{R1} \Big/ \sum_m T_m$	46	—

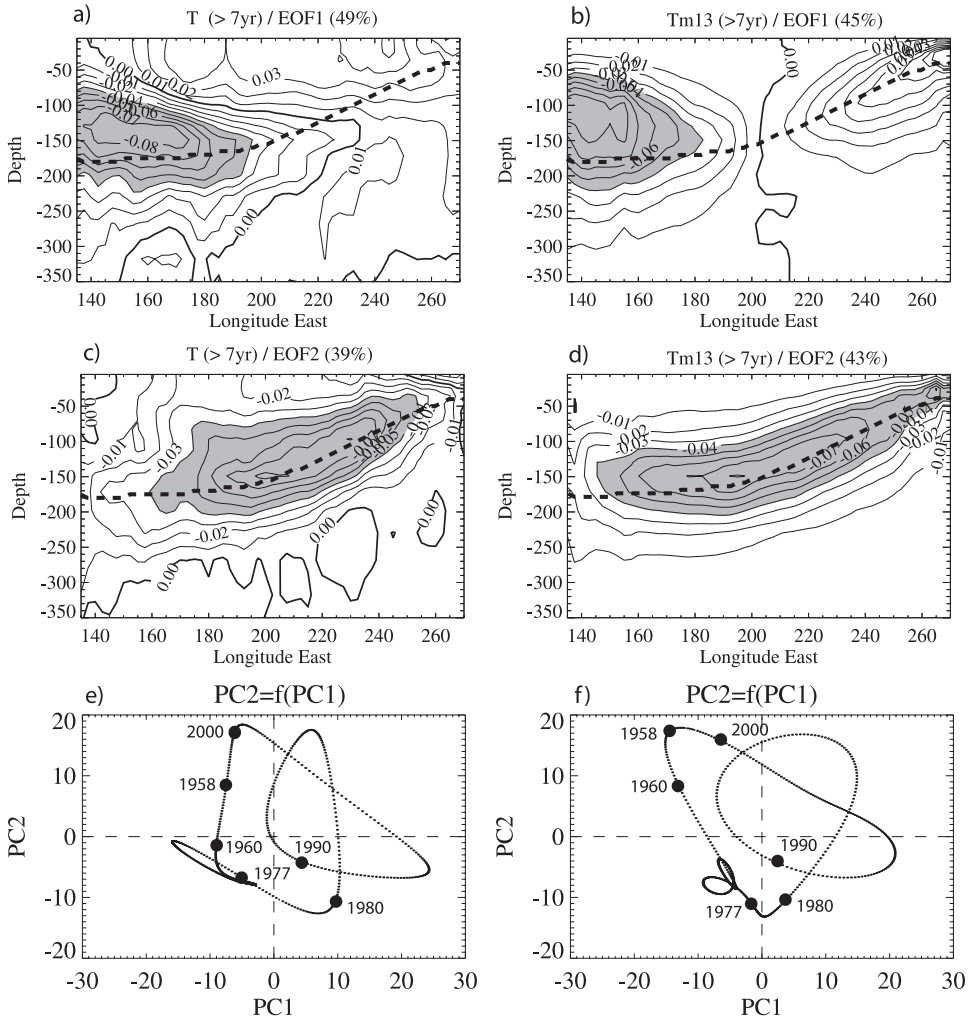

FIG. 3. Spatial pattern associated with the EOF modes (top) 1 and (middle) 2 of the 7-yr low-pass-filtered temperature along the equator for (a),(c) SODA and (b),(d) the contribution of baroclinic modes 1–3. The contour interval is 0.01°C. Shading is for anomalies smaller than −0.04°C. (bottom) The scattered plot of the second PC2 time series as a function of the PC2 time series for (e) SODA and (f) the contribution of modes 1–3. Values of the PCs for the contribution of modes 1–3 were multiplied by 1.5. The thick dashed line in (a)–(d) represents the mean thermocline depth.

value of the explained variance of the first two dominant modes and calculating the spatial correlation over the domain (130°–270°E; 0–350 m) between the EOF modes of the original field (Fig. 3) and the ones of the scrambled dataset. We find that 90% of the ensemble leads to a correlation higher than 0.96 (0.88) for the first (second) EOF mode, which demonstrates the robustness of the EOF patterns of Fig. 3.

Notice that the first EOF mode of SODA and $\sum_{m=1}^{3} T_m$ closely resemble the temperature pattern associated with the 1976 climate shift (Figs. 1, 2a). The percentage of explained variance of the first mode is also comparable (49% versus 45%), indicating that the first three baroclinic mode contributions do grasp similar variability characteristics than the "full" SODA data. Similar observations can be made for the second EOF mode: SODA and $\sum_{m=1}^{3} T_m$ have a similar pattern and percentage of explained variance. Their associated time series correlates at 0.91 (0.90) for mode 1 (mode 2). The amplitude of $\sum_{m=1}^{3} T_m$ is, however, less than in SODA by an average factor of ~1.5 [ratio of the variance of the principal component (PC) time series]. Note that, to ease the comparison between SODA and the modal decomposition, the values of PC1 and PC2 for $\sum_{m=1}^{3} T_m$ were multiplied by 1.5 to derive the scattered plot of Fig. 3f.

These results first indicate that the 1976 climate shift pattern for temperature (Fig. 1) is associated with the dominant mode for decadal temperature variability along

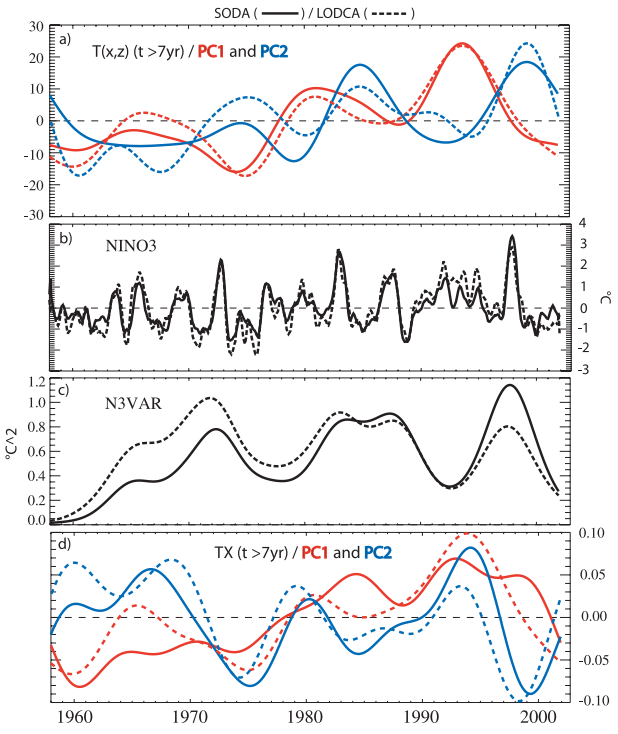

FIG. 4. (a) PC time series of EOF1 (red) and EOF2 (blue) modes of the 7-yr low-pass-filtered vertical temperature for SODA (solid) and LODCA (dashed). (b) Niño-3 SST index for SODA and LODCA; a 5-month running mean was applied. (c) N3VAR index for SODA and LODCA. (d) PC time series of EOF1 (red) and EOF2 (blue) modes of the 7-yr low-pass-filtered zonal wind stress anomalies for SODA and LODCA.

the equator, which is consistent with the characteristics of PC1 (cf. Fig. 4a)—namely, a clear signature of the transition from warm to cold in 1977 (''warm'' and ''cold'' here refer to the temperature in the Niño-4z region). This mode consists of a cooling in the vicinity of the thermocline in the warm pool region during periods of warm SST and a warming in the surface layer in the eastern Pacific. Except for the surface layer, the mode is associated to a large extent with the variability of the first three baroclinic modes and corresponds to the change in the slope of the mean thermocline associated with the 1976/77 climate shift. The second mode of temperature variability at a decadal time scale along the equator is distinct from the 1976 climate shift pattern and mostly corresponds to a basinwide uplift of the mean thermocline. It has a larger zonal extent than the first mode and explains a significant amount of variance (39% for SODA and 43% for $\sum_{m=1}^{3} T_m$). It is behind the first mode by 5 yr (maximum correlation between PC1 and PC2 reaches 0.76 at lag = 5 yr; cf. Fig. 4). The phase relationship between PC1 and PC2 is further investigated through the scatter diagrams between PC1 and PC2 presented in Figs. 3e,f for SODA and $\sum_{m=1}^{3} T_m$, respectively. The comparison between the two PCs indicates an overall good agreement, which means that the first three baroclinic modes do grasp the dynamics of the decadal mode. Also notice the change in the relationship between PC1 and PC2 at the transition of the 1976/77 climate shift, which may traduce the change in ENSO characteristics (the smaller amplitude range of the PC1 and PC2 prior to 1977 and an overall more ''cyclic trajectory'' after 1977).

4. Link with ENSO variability

We now investigate the relationship between the 1976 climate shift pattern for temperature and the ENSO variability. As a first step, an EOF analysis is carried out on the interannual anomaly of the temperature field along the equator in the first 300 m. A bandpass filter in the 2–7 $(\text{yr})^{-1}$ frequency band was used to focus on ENSO time scales. Figure 5 presents the results for the first two modes that grasp more than 95% of the explained variance. The first mode of SODA corresponds to the ENSO mode, with a warming/cooling in the eastern Pacific in the first 100 m and a cooling/warming in the far western Pacific. The first EOF mode of the first three baroclinic modes ($\sum_{m=1}^{3} T_m$) also exhibits a zonal seesaw: warm in the east and cold in the west, with the pivot located at the date line. The associated times series of the first mode for SODA and $\sum_{m=1}^{3} T_m$ are highly correlated ($c = 0.92$). However, the warm anomaly pattern in the east is less intense in $\sum_{m=1}^{3} T_m$ than in SODA and consists of a ''beam'' sloping eastward and downward from the surface at the eastern boundary, indicative of vertical propagation of energy at interannual time scales (Dewitte and Reverdin 2000). Note that T_m only accounts for the temperature anomaly associated with vertical displacements of the isotherm, which has the effect of emphasizing the vertical propagation of the temperature anomaly. In the west, the amplitude of the EOF mode for $\sum_{m=1}^{3} T_m$ is similar to that of SODA, indicating that the temperature changes in this region can be interpreted as vertical displacements of the isotherms.

Despite the differences for the first EOF mode between SODA and $\sum_{m=1}^{3} T_m$, the second modes for both SODA and $\sum_{m=1}^{3} T_m$ strikingly exhibit a spatial pattern that shares many characteristics with the first EOF mode of decadal temperature [Figs. 3a,b; also with the 1976 climate shift pattern (Fig. 1)]. The pattern of the second EOF modes for both SODA and $\sum_{m=1}^{3} T_m$ extends somewhat farther to the east (following the mean thermocline depth) compared to the first EOF of Figs. 3a,b, which also mimics the pattern of the second EOF mode for decadal temperature (Figs. 3c,d). The correlation between the time series associated with the second EOF mode for SODA and

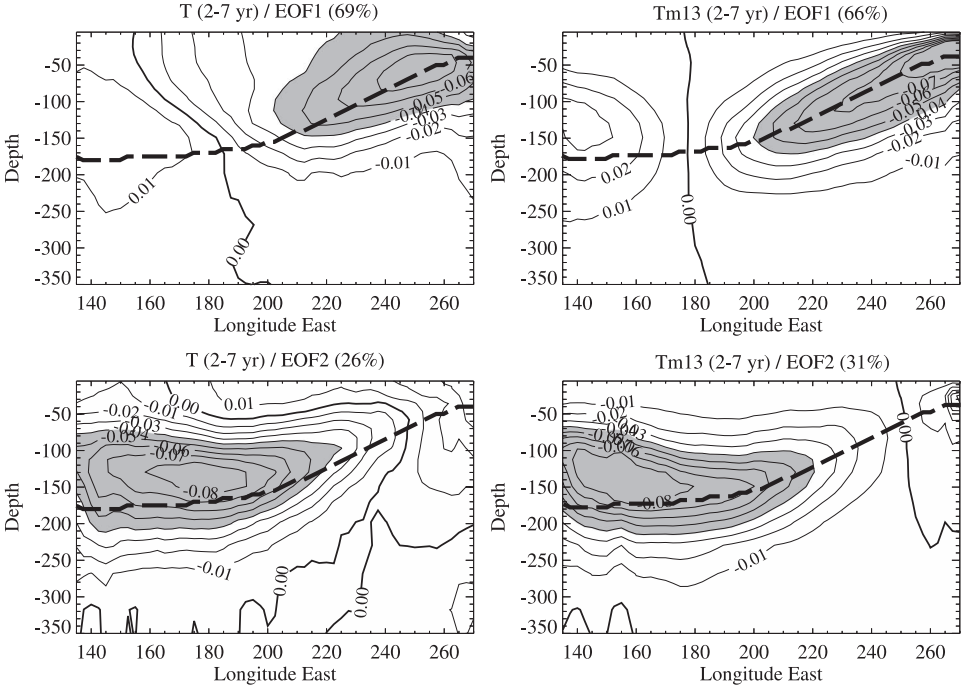

FIG. 5. Same as in Fig. 3, but for the interannual variability [i.e., data were previously bandpass filtered for frequencies between 2 and 7 $(\text{yr})^{-1}$]. The thick dashed line represents the mean thermocline depth.

$\sum_{m=1}^{3} T_m$ reaches 0.87. Note that similar results are obtained without filtering the temperature anomaly field.

This similarity suggests a link between the decadal mode of temperature along the equator and the interannual variability. As a matter of fact, the values of correlation between the time series of the first two EOF modes of decadal temperature for SODA (Fig. 4a) and classical indices of ENSO variability are large, significant at the 95% level (see Table 2). As a reference, Table 2 also provides the correlation between the Pacific decadal oscillation (PDO) index and the EOF time series.

Interestingly, the first EOF mode for decadal temperature variability leads the ENSO modulation index (N3VAR index by ~4 yr but is in phase with the Niño-3 SST index [SST averaged in the Niño-3 region (5°S–5°N, 150°–90°W; cf. Fig. 4b)] that has been low-pass filtered with a frequency cutoff at 7 yr, which is consistent with the idea that ENSO modifies the mean state, which in turn rectifies the ENSO variability. In particular, Dewitte et al. (2007) showed that this process operates through the redistribution of energy of the first three baroclinic modes when the mean thermocline fluctuates in the western-central Pacific. On the other hand, the second EOF mode is behind the N3VAR index by ~1 yr, suggesting that the basinwide change in thermocline depth (Fig. 3c) is driven by changes in ENSO dynamics, resulting from a change in mean state in the western Pacific [the first EOF (EOF1)]. The N3VAR index is displayed in Fig. 4c.

To investigate further the possibility of interaction between interannual and decadal time scales, the skewness of vertical temperature along the equator is estimated. Indeed, because ENSO is skewed, the decadal growth of the ENSO amplitude can be translated into decadal background state changes (An 2008). Hence, decadal tropical variability is a residuum of the skewed ENSO amplitude modulations. This idea had been supported by Timmermann (2003) and Rodgers et al. (2004) using a CGCM simulation. Figure 6 presents the results for

TABLE 2. Maximum lag correlation between the time series of EOF1 and EOF2 of decadal temperature for SODA and classical indices of ENSO variability. Parentheses indicate lags in months. Positive lags correspond to the EOF mode leading the index. Correlation values above 0.64 are significant at the 95% confidence level.

	SODA EOF1 (f-7yr)	SODA EOF2 (f-7yr)
N3VAR[a]	0.79 (46)	0.81 (−15)
WWV (f-7 yr)[b]	−0.92 (44)	−0.83 (−10)
PDO[c]	0.71 (14)	0.41 (−42)

[a] Scale-averaged wavelet power over the (2–7) years of the Niño-3 SST index (cf. Cibot et al. 2005).

[b] A 7-yr low-pass-filtered warm water volume index in the equatorial Pacific calculated as in Meinen and McPhaden (2001), which corresponds to the spatial integration of 20°C isotherm along (5°N–5°S , 120°E–80°W).

[c] PDO index calculated from SODA SST following Hare and Mantua (2000) (7-yr low-pass filtered).

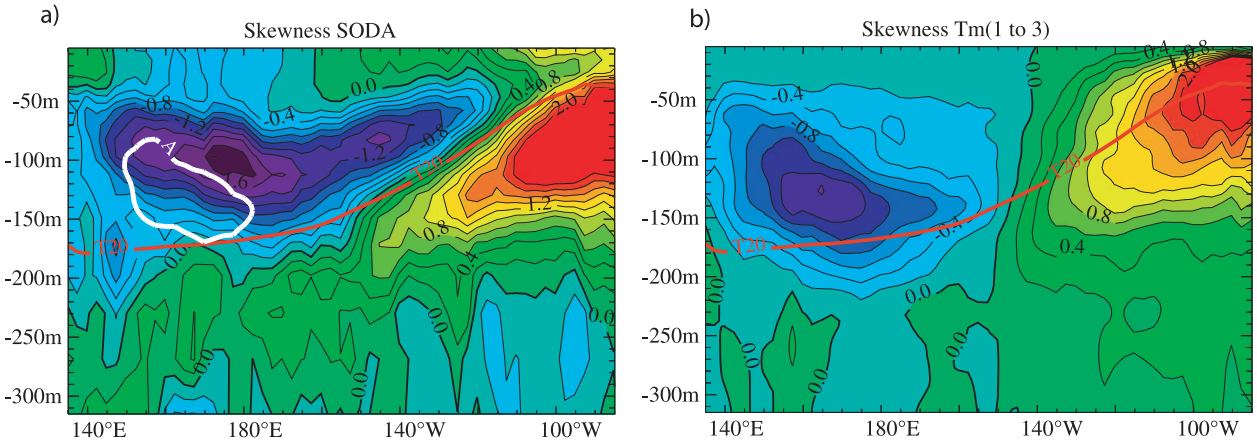

FIG. 6. Weighted skewness of temperature as a function of depth along the equator for (a) SODA and (b) for contribution of modes 1–3. The weighted skewness is defined as m_3/m_2, where $m_k = \sum_{i=1}^{N}(x_i-\bar{x})^k/N$; x_i is the ith observations, $\bar{x}$ the mean, and N the number of observations. Units are in °C. The mean 20°C isotherm depth is shown in red. The white contour (labeled A) in (a) represents the contour of −1.°C skewness of (b).

SODA and $\sum_{m=1}^{3} T_m$. Interestingly, SODA exhibits a zone of negative skewness peaking around ~100 m in the western-central Pacific. Positive skewness in the far eastern Pacific corresponds to the classical view of ENSO asymmetry, namely, a stronger El Niño event than a La Niña event (see Fig. 3 of An 2008). Here $\sum_{m=1}^{3} T_m$ also exhibits a zone of negative skewness in the western Pacific just above the thermocline. However, compared to SODA, this zone is displaced to the west and is deeper (~150 m; see white contour in Fig. 6a). It better fits the decadal mode of temperature for SODA (cf. Figs. 3a or 1). The ''peak'' of negative skewness of SODA in the ~110-m-depth range (Fig. 6a) is likely to be associated with the contribution of higher-order baroclinic modes that can grasp variability that may originate from the off-equatorial region. On the other hand, the pattern of skewness for $\sum_{m=1}^{3} T_m$ (Fig. 6b) has a minimum value in the zone of mean change in temperature, which supports the hypothesis that the decadal mode results from the residual effect of the asymmetric ENSO variability. Consistently with this interpretation, the second EOF mode (EOF2) of the interannual temperature anomaly (Fig. 5c), which has a pattern that compares better to the skewness pattern of $\sum_{m=1}^{3} T_m$ than SODA ($T > 7$ yr), is skewed. The skewness value of the associated time series is 10 times larger than the skewness associated to the first EOF time series.

5. Discussion and conclusions

We have shown from the SODA reanalysis that temperature change at decadal time scales in the western-central Pacific can be explained by vertical displacements of the isotherms associated to the gravest baroclinic modes: 67% of the variance of temperature change at decadal time scale in the vicinity of the equatorial thermocline (Niño-4z region defined as the zone encompassing 150°E–150°W; 100–150 m) can be explained by the first three baroclinic modes. This variability corresponds to a large extent to the Kelvin and first meridional Rossby waves activity. Consistent with Moon et al. (2004), such a variability pattern is related to the ENSO modulation with the change in mean state, represented as EOF1 of the low-frequency vertical temperature (Fig. 3a), leading the change in ENSO characteristics. The EOF2 mode of the low-frequency vertical temperature accounts also for a significant variance of the decadal variability (39% and 43% for SODA and $\sum_{m=1}^{3} T_m$, respectively) and is associated with basinwide changes in mean thermocline that follow the ENSO modulation. (Fig. 3c; Table 2). The results also indicate that the vertical temperature in the vicinity of the mean thermocline in the western-central Pacific (Niño-4z region) is negatively skewed. The pattern of skewness for the first three baroclinic mode contributions to temperature anomaly suggests that the asymmetry of the ENSO cycle translates to the decadal mode in the Niño-4z region. In other words, the ENSO modulation associated with the change in mean state along the equator is related to the asymmetry of the ENSO cycle in the western-central Pacific at the subsurface. Because the asymmetry pattern is recovered in the temperature anomaly field recomposed from the first three baroclinic modes, it has to result directly from wind forcing. To estimate to what extent the wind forcing is associated with the asymmetry of temperature in the vicinity of the thermocline described in this paper (Figs. 6a,b), a linear model is forced using the ERA-40 winds and the outputs are analyzed in a similar way as for

SODA. The linear model is the same used by Dewitte (2000), named LODCA, but tuned with the wind projection coefficients and the values for phase speed as derived from the vertical mode decomposition of the mean SODA stratification at 160°W along the equator ($P_1 = 0.61$, $P_2 = 0.51$, $P_3 = 0.16$, $c_1 = 2.67$ m s^{-1}, $c_2 = 1.58$ m s^{-1}, $c_3 = 1.00$ m s^{-1}). Note that the linear model simulates a Niño-3 SST (N3VAR) index that correlates at the 85% (79%) level with SODA during the period 1958–2001 (Figs. 4b,c). To recompose the baroclinic temperature from the simulated baroclinic contributions to sea level anomaly, the zonally varying mean vertical mode profiles from SODA are used to take into account the sloping mean thermocline from west to east. Although the linear model resolves a large number of meridional modes for the Rossby waves, only the Kelvin and first meridional Rossby wave contributions to sea level anomalies are considered to derive the baroclinic temperature. Figure 7 presents the results for the control run and another experiment that consists of cancelling out the reflections at the meridional bounbaries while running the model to ''filter out'' the impact of free-propagating reflected waves on temperature change. This latter experiment is aimed at inferring what is directly induced by the local wind forcing. The experiments are referred as LODCA-CR and LODCA-Roff, respectively. Interestingly, both simulations exhibit similar pattern for skewness of interannual baroclinic temperature, which compare to some extent to the results of the modal decomposition of SODA (Fig. 5b). The magnitude of the ''patches'' of negative skewness in the western-central Pacific around ~130 m are also comparable to the linear model simulations and to the modal decomposition of SODA, which indicates that such a pattern is mostly forced by the winds and may not result only from nonlinear processes associated with thermocline dynamics. Notice that the decadal mode for baroclinic temperature in the LODCA-CR simulation (Figs. 7c,e) shares many characteristics with the one derived from SODA (Figs. 3b,d); however, for the first (second) EOF mode, the longitude of the pivot of the zonal seasaw (of the peak amplitude) is displaced ~30° to the west compared to SODA. This is believed to be due to the tendency of the linear model to overestimate the reflections at the meridional boundaries and the simplified formulation for friction used to model the dissipation of the waves. Despite the discrepancies between LODCA-CR and SODA, the distribution of explained variance onto the first two EOF modes is comparable between the linear simulation and SODA, and their associated time series are highly correlated (0.75 and 0.94 for the PC1 and PC2, respectively; cf. Fig. 4a). On the other hand, for LODCA-Roff, the dominant decadal mode of baroclinic temperature (Fig. 7d) is different from the one of SODA—in particular, the weaker variability in the western Pacific—the peak of which is displaced westward compared to LODCA-CR. This indicates that there is a significant contribution of the reflected Rossby waves to the change in mean state in the Niño-4z region, which is consistent with the modal decomposition of SODA (Table 1). The second EOF in LODCA-Roff (Fig. 7f) is less energetic and grasps similar low-frequency variability than the one of the first EOF mode of SODA.

These results corroborate the interpretation of subsurface temperature variability in SODA proposed in this paper, namely, a linear response to the wind forcing that involves high-order baroclinic modes (modes 1–3). To infer what in the winds is leading to such variability, an EOF analysis is performed on the low-pass-filtered ERA-40 wind stress anomalies (both zonal and meridional components are considered). The results are presented in Figs. 8a,b for zonal wind stress. The first mode corresponds to the transition mode from ''cold'' to ''warm'' of the 1976/77 shift (see PC1 on Fig. 4d), with a relatively uniform zonal structure over the central Pacific corresponding to an increase/decrease of the mean trade winds. The correlation between its associated time series and the PC time series of the first EOF mode of decadal temperature variability (Fig. 4a, solid red line) reaches 0.80. The second EOF (Fig. 8b) has an equatorial zonal seasaw structure. The correlation between its associated time series and the PC time series of the second EOF mode of decadal temperature variability (Fig. 4a, solid blue line) reaches −0.57. Although slightly displaced to the west, this EOF mode resembles the linear response of a Gill-type model (Gill 1980) to El Niño–type (La Niña) SST anomalies, namely, westerlies (easterlies) in the western (eastern) equatorial Pacific. Actually, the first EOF mode (Fig. 8a) could also be interpreted as a linear response of the tropical atmospheric circulation to ENSO-like anomalies that would be displayed slightly to the east. To support this interpretation, a similar EOF analysis was performed on the wind stress anomalies simulated by LODCA. Note that LODCA is a coupled model (that uses a Gill atmosphere; cf. Dewitte 2000). Thus, the simulated wind stress anomalies result here from the forcing of the atmosphere by the simulated SST anomalies, which compare to some extend to the SODA SST (see Fig. 4b). The results are displayed in the Figs. 8c,d for the spatial patterns of the first two dominant modes and in Fig. 4d for the associated time series. Whereas the correlation values between the PC time series of SODA and LODCA reach 0.77 and 0.74 for modes 1 and 2, respectively, the spatial patterns of the EOFs have comparable zonal structures. It indicates that LODCA grasps some aspects of the decadal

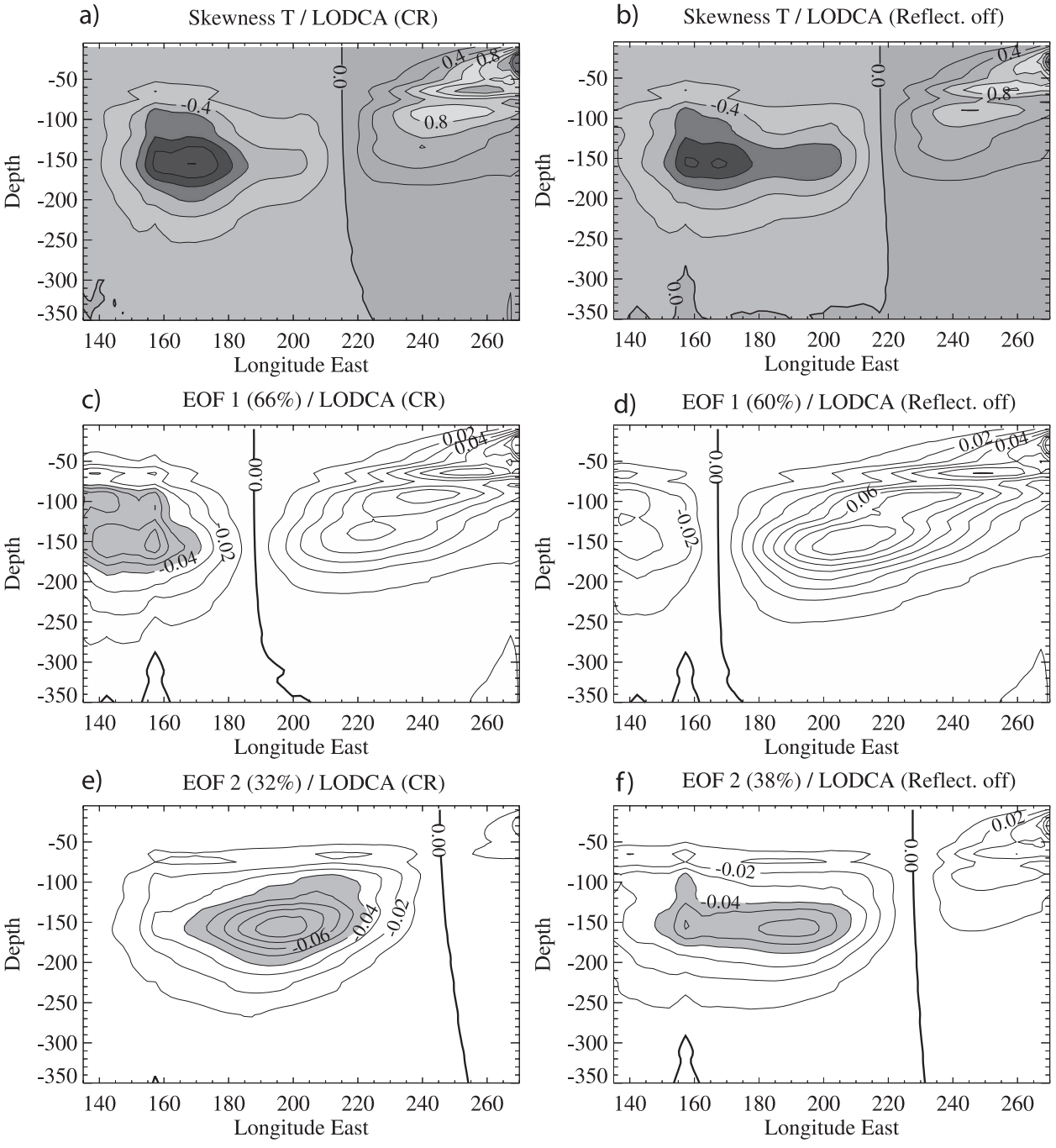

FIG. 7. Results of the linear model experiments: (a),(b) Skewness of baroclinic temperature and (c)–(f) EOF1 and EOF2 (spatial pattern) of its low-frequency component (A 7-yr low-pass filter is applied on $\sum_{m=1}^{3} T_m$) along the equator and as a function of depth; (left) LODCA-CR and (right) LODCA-Roff (see text). Units are in °C for skewness. The PC time series associated with the EOF1 and EOF2 for LODCA-CR are displayed in Fig. 4a (dashed lines).

modes observed in the ERA-40 winds. Differences between ERA-40 and LODCA can originate from the simplified physics of the intermediate coupled model and from the inability of the EOF analysis to separate the first two modes as clearly in LODCA as in SODA (see PC time series in Fig. 4d). It could also be because low-frequency change in mean stratification is not considered in LODCA (since the P_n parameters are prescribed and fixed). In particular, Dewitte et al. (2007) show that the latter model may make a substantial

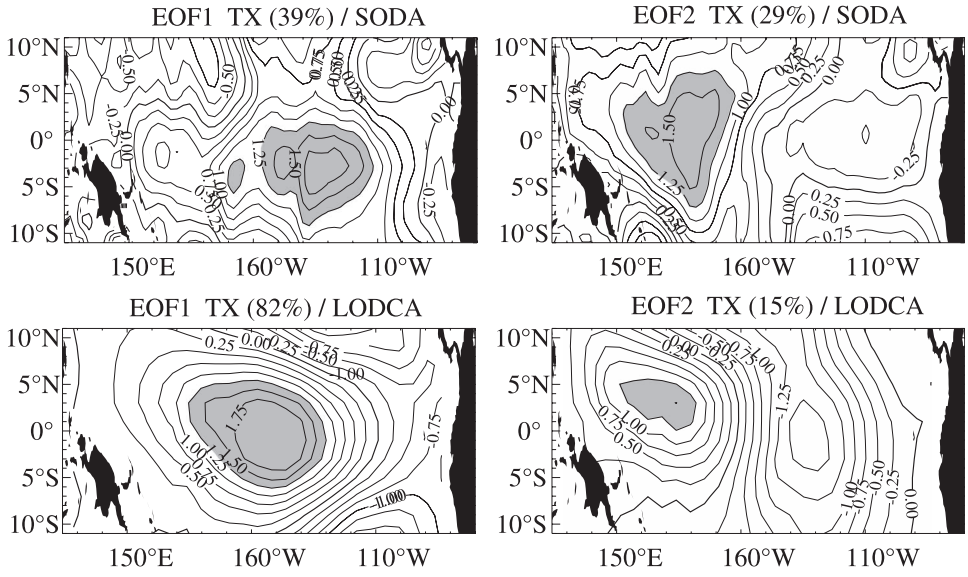

FIG. 8. EOF1 and EOF2 of the decadal zonal wind stress anomalies for (top) SODA and (bottom) LODCA. Associated time series are displayed in Fig. 4d. EOF2 for LODCA was multiplied by 2 to ease the comparison.

contribution to the decadal mode in the tropical Pacific. Nevertheless, it is striking that, within the simplified model setup proposed here, such an agreement between model and ''observations'' can be reached for the atmospheric response. Although the influence of the extratropics on the tropical atmospheric circulation cannot be excluded, our results are consistent with the hypothesis of a tropical mechanism for change in mean state that results from the residual effect of the asymmetric ENSO variability. In that sense, it is consistent with the observational study by An (2004) and other modeling studies (Rodgers et al. 2004; Dewitte et al. 2007) that mostly focus on surface data. Here, we extend these works, focusing on the role of subsurface temperature variability. As a final quantitative consistency check on the SODA outputs, a singular value decomposition (SVD) analysis between the running skewness of SST (x, y) (between 10°N and 10°S) and the running mean of $\sum_{m=1}^{3} T_m(x, z)$ for SODA was carried out to extract the significant statistical relationship between the ENSO asymmetry and the low-frequency change in stratification in the vicinity of the thermocline. A running windows spanning 7 yr was used. The results are consist with a dominant mode, explaining 83% of the covariance with patterns for SST and $\sum_{m=1}^{3} T_m$ resembling, strikingly, the patterns of skewness of SST anomalies and the first EOF of the decadal mode of $\sum_{m=1}^{3} T_m$ (not shown). Although there is some limitation owned to the relatively short record of SODA for such calculation, it supports the above interpretation.

Overall, our results suggest that the realism of decadal variability as simulated by coupled models may be critically dependent on how both the ENSO asymmetry and the vertical structure variability are reproduced in these models. Notice there is a large diversity of behavior of the current CGCMs with regard to the ENSO asymmetry (An et al. 2005) and the decadal variability/ENSO modulation (Lin 2007). This may have implications for our ability to predict and understand the response of the climate to global warming, because the temperature at the subsurface contains the memory of the tropical Pacific system and may respond with a delay to the increasing greenhouse gases. Our results suggest that the warm pool region at the subsurface may behave as a ''thermostat'' to a warmer climate. This is a topic of current research using the Intergovernmental Panel on Climate Change (IPCC) Fourth Assessment Report (AR4) CGCMs.

Acknowledgments. The authors thank Axel Timmermann for stimulating discussions during the ENSO workshop ''Exploring El Niño: Beyond the current understanding and predictability barrier'' in Seoul on 12–13 September 2006. Soon-Il An, Sang-Wook Yeh, Byung-Kwon Moon, and Boris Dewitte benefited from support of the Centre National de la Recherche Scientifique (CNRS) through a Science and Technology Amicable Research (STAR) program. S.-I. An was supported from the ''National Comprehensive Measures against Climate Change'' program by the Ministry of Environment, Korea (Grant 1600-1637-301-210-13). Sulian Thual benefited from support of Institut de Recherche pour le Développement (IRD) and the Agence National de la Recherche (ANR) within the Peru

Chile Climate Change (PCCC) project while visiting the Instituto del Mar del Peru, Callao (IMARPE).

REFERENCES

Adler, R. F., and Coauthors, 2003: The Version-2 Global Precipitation Climatology Project (GPCP) monthly precipitation analysis (1979–present). *J. Hydrometeor.,* **4,** 1147–1167.

An, S.-I., 2004: Interdecadal changes in the El Nino-La Nina asymmetry. *Geophys. Res. Lett.,* **31,** L23210, doi:10.1029/2004GL021699.

——, 2008: A review on interdecadal changes in the nonlinearity of the El Niño-Southern Oscillation. *Theor. Appl. Climatol.,* **97,** 29–40.

——, and F.-F. Jin, 2004: Nonlinearity and asymmetry of ENSO. *J. Climate,* **17,** 2399–2412.

——, Y.-G. Ham, J.-S. Kug, F.-F. Jin, and I.-S. Kang, 2005: El Niño–La Niña asymmetry in the coupled model intercomparison project simulations. *J. Climate,* **18,** 2617–2627.

Björnsson, H., and S. A. Venegas, 1997: A manual for EOF and SVD analyses of climatic data. McGill University CCGCR Rep. 97-1, 52 pp.

Blanke, B., J. D. Neelin, and D. Gutzler, 1997: Estimating the effect of stochastic wind stress forcing on ENSO irregularity. *J. Climate,* **10,** 1473–1486.

Burgman, R. J., P. S. Schopf, and B. P. Kirtman, 2008: Decadal modulation of ENSO in a hybrid coupled model. *J. Climate,* **21,** 5482–5500.

Carton, J. A., and B. S. Giese, 2008: A reanalysis of ocean climate using Simple Ocean Data Assimilation (SODA). *Mon. Wea. Rev.,* **136,** 2999–3017.

——, G. Chepurin, X. Cao, and B. S. Giese, 2000: A Simple Ocean Data Assimilation analysis of the global upper ocean 1950–95. Part I: Methodology. *J. Phys. Oceanogr.,* **30,** 294–309.

Cibot, C., E. Maisonnave, L. Terray, and B. Dewitte, 2005: Mechanisms of tropical Pacific interannual-to-decadal variability in the ARPEGE/ORCA global coupled model. *Climate Dyn.,* **24,** 823–842.

Conkright, M. E., and Coauthors, 2002: *Introduction*. Vol. 1, *World Ocean Database 2001,* NOAA Atlas NESDIS 42, 159 pp.

Dewitte, B., 2000: Sensitivity of an intermediate coupled ocean–atmosphere model of the tropical Pacific to its oceanic vertical structure. *J. Climate,* **13,** 2363–2388.

——, and G. Reverdin, 2000: Vertically propagating annual and interannual variability in an OGCM simulation of the tropical Pacific in 1985–94. *J. Phys. Oceanogr.,* **30,** 1562–1581.

——, ——, and C. Maes, 1999: Vertical structure of an OGCM simulation of the equatorial Pacific Ocean in 1985–94. *J. Phys. Oceanogr.,* **29,** 1542–1570.

——, S.-W. Yeh, B.-K. Moon, C. Cibot, and L. Terray, 2007: Rectification of the ENSO variability by interdecadal changes in the equatorial background mean state in a CGCM simulation. *J. Climate,* **20,** 2002–2021.

Dukowicz, J. K., and R. D. Smith, 1994: Implicit free-surface method for the Bryan-Cox-Semtner ocean model. *J. Geophys. Res.,* **99,** 7991–8014.

Giese, B. S., S. C. Urizar, and N. S. Fučkar, 2002: Southern Hemisphere origins of the 1976 climate shift. *Geophys. Res. Lett.,* **29,** 1–4.

Gill, A. E., 1980: Some simple solutions for heat-induced tropical circulation. *Quart. J. Roy. Meteor. Soc.,* **106,** 447–462.

——, 1982: *Atmosphere-Ocean Dynamics*. International Geophysics Series, Vol. 30, Academic Press, 662 pp.

Gu, D., and S. G. H. Philander, 1997: Interdecadal climate fluctuations that depend on exchanges between the tropics and extratropics. *Science,* **275,** 805–807.

Guilderson, T. P., and D. P. Schrag, 1998: Abrupt shift in subsurface temperatures in the eastern tropical pacific associated with recent changes in El Niño. *Science,* **281,** 240–243.

Hare, S. R., and N. J. Mantua, 2000: Empirical evidence for North Pacific regime shifts in 1977 and 1989. *Prog. Oceanogr.,* **47,** 103–146.

Illig, S., and B. Dewitte, 2006: Local coupled equatorial variability versus remote ENSO forcing in an intermediate coupled model of the tropical Atlantic. *J. Climate,* **19,** 5227–5252.

Jin, F.-F., 2001: Low-frequency modes of tropical ocean dynamics. *J. Climate,* **14,** 3874–3881.

Lin, J.-L., 2007: Interdecadal variability of ENSO in 21 IPCC AR4 coupled GCMs. *Geophys. Res. Lett.,* **34,** L12702, doi:10.1029/2006GL028937.

Luo, J.-J., and T. Yamagata, 2001: Long-term El Nino-Southern Oscillation (ENSO)-like variation with special emphasis on the South Pacific. *J. Geophys. Res.,* **106,** 22 211–22 227.

——, S. Masson, S. Behera, P. Delecluse, S. Gualdi, A. Navarra, and T. Yamagata, 2003: South Pacific origin of the decadal ENSO-like variation as simulated by a coupled GCM. *Geophys. Res. Lett.,* **30,** 2250, doi:10.1029/2003GL018649.

Meinen, C. S., and M. J. McPhaden, 2001: Interannual variability in warm water volume transports in the equatorial Pacific during 1993–99. *J. Phys. Oceanogr.,* **31,** 1324–1345.

Moon, B.-K., S.-W. Yeh, B. Dewitte, J.-G. Jhun, I.-S. Kang, and B. P. Kirtman, 2004: Vertical structure variability in the equatorial Pacific before and after the Pacific climate shift of the 1970s. *Geophys. Res. Lett.,* **31,** L03203, doi:10.1029/2003GL018829.

——, ——, ——, ——, and ——, 2007: Source of low frequency modulation of ENSO amplitude in a CGCM. *Climate Dyn.,* **29,** 101–111.

Pierce, D. W., T. P. Barnett, and M. Latif, 2000: Connections between the Pacific Ocean tropics and midlatitudes on decadal timescales. *J. Climate,* **13,** 1173–1194.

Rodgers, K. B., P. Friederichs, and M. Latif, 2004: Tropical Pacific decadal variability and its relation to decadal modulation of ENSO. *J. Climate,* **17,** 3761–3774.

Schopf, S. P., and R. J. Burgman, 2006: A simple mechanism for ENSO residuals and asymmetry. *J. Climate,* **19,** 3167–3179.

Smith, R. D., J. K. Dukowicz, and R. C. Malone, 1992: Parallel ocean general circulation modeling. *Physica D,* **60,** 38–61.

Timmermann, A., 2003: Decadal ENSO amplitude modulations: A nonlinear paradigm. *Global Planet. Change,* **37,** 135–156.

——, and F.-F. Jin, 2002: A nonlinear mechanism for decadal El Niño amplitude changes. *Geophys. Res. Lett.,* **29,** 1003, doi:10.1029/2001GL013369.

Uppala, S. M., and Coauthors, 2005: The ERA-40 Re-Analysis. *Quart. J. Roy. Meteor. Soc.,* **131,** 2961–3012.

Wang, B., and S.-I. An, 2001: Why the properties of El Niño changed during the late 1970s. *Geophys. Res. Lett.,* **28,** 3709–3712.

Yeh, S.-W., and B. P. Kirtman, 2004: Tropical Pacific decadal variability and ENSO amplitude modulation in a CGCM. *J. Geophy. Res.,* **109,** C11009, doi:10.1029/2004JC002442.

——, and ——, 2008: Internal atmospheric variability and interannual-to-decadal ENSO variability in a CGCM. *J. Climate,* **22,** 2335–2355.

——, B. Dewitte, J.-G. Jhun, and I.-S. Kang, 2001: The characteristic oscillation induced by coupled processes between oceanic vertical modes and atmospheric modes in the tropical Pacific. *Geophys. Res. Lett.,* **28,** 2847–2850.